The Melting Layer: A Laboratory Investigation of Ice Particle Melt and Evaporation near 0°C

R. G. ORALTAY

Environmental Engineering Department, Engineering Faculty, Marmara University, Ziverbey, Istanbul, Turkey

J. HALLETT

Desert Research Institute, Reno, Nevada

(Manuscript received 26 December 2003, in final form 25 July 2004)

ABSTRACT

Melting, freezing, and evaporation of individual and aggregates of snow crystals are simulated in the laboratory under controlled temperature, relative humidity, and air velocity. Crystals of selected habit are grown on a vertical filament and subsequently melted or evaporated in reverse flow, with the velocity adjusted for appropriate fall speed to reproduce conditions of the melting layer. Nonequilibrium conditions are simulated for larger melting ice particles surrounded by smaller drops at a temperature up to +5°C or growth of an ice crystal surrounded by freezing ice particles down to −5°C. Initial melting of well-defined faceted crystals, as individuals or in combination, occurs as a water layer >10 μm thick. For larger (>100 μm) crystals the water becomes sequestered by capillary forces as individual drops separated by water-free ice regions, often having quasiperiodic locations along needles, columns, or arms from evaporating dendrites. Drops are also located at intersections of aggregate crystals and dendrite branches, being responsible for the maximum of the radar scatter. The drops have a finite water–ice contact angle of 37°–80°, depending on ambient conditions. Capillary forces move water from high-curvature to low-curvature regions as melting continues. Toward the end of the melting process, the ice separating the drops becomes sufficiently thin to fracture under aerodynamic forces, and mixed-phase particles are shed. Otherwise ice-free drops are shed. The melting region and the mechanism for lowering the melting layer with an increasing precipitation rate are associated with smaller ice particle production capable of being lofted in weaker updrafts.

1. Introduction: The melting layer

As snow crystals nucleate, grow aloft, and fall to lower levels, changing conditions of relative humidity and temperature influence their evolution. Further growth by riming or from vapor, evaporation, aggregation, and ultimately melting takes place as the environmental wet-bulb temperature rises above 0°C. Much can happen during these processes, not the least being the increasing concentration of crystals from evaporation breakup and Hallett–Mossop secondary ice production, should riming conditions be favorable. Further, as demonstrated by Stewart (1984) and Stewart et al. (1984) and others, near-saturated isothermal layers at 0°C may develop and deepen as snow continues to fall, to condition such air by cooling through evaporation and melting, resulting in a gradual lowering of the region of the melting level. Thus specification of the ice particles entering the melt region is a formidable undertaking even in the absence of any vertical motion and differential horizontal advection (Clough and Franks 1991; Clough et al. 2000). Any attempt at prediction and interpretation of radar reflectivity will depend critically on an ability to determine the larger particle characteristics, through changing aggregation by mechanical entanglement and contact sticking. The habit of the crystals forming such aggregates responds to the temperature and supersaturation of vapor growth (Hallett and Mason 1958; Bailey and Hallett 2002) and the levels where vertical motion provide such an opportunity. Models of the melting region itself must incorporate this level of detail (Szyrmer and Zawadzki 1999; Fabry and Szyrmer 1999). Similar considerations apply to larger mixed-phase particles as they fall to temperature levels a few degrees above 0°C, leading to the maximum reflectivity of the radar bright band (Drummond et al. 1996 and others). Earlier experimental work by the present authors (Oraltay and Hallett 1989) shows that complicated phenomena occur when ice particles melt, dependent on the original ice

Corresponding author address: J. Hallett, 2215 Raggio Pkwy., Reno, NV 89512.
E-mail: John.Hallett@dri.edu

habit, capable of determining the spatial distribution of water over the complicated matrix of the snowflake. Such melting effects ultimately lead to a decrease in particle size, increasing fall velocity, and the consequent decrease in particle concentration, as the signal reduction below the radar bright band is conventionally explained. The reality is even more complicated. We here extend the previous experimental studies to investigate the detail of the physical processes leading to particle melt and their dependence on particle habit composition, determined earlier during growth. There is a dependence on nonequilibrium brought about by a spread in the ice particle size distribution and the resulting lag times of melting; larger melting particles responsible for the maximum of the melting layer radar echo may be surrounded by completely melted particles having a temperature several degrees higher. The ultimate question to be addressed is whether there is an explanation in terms of a unique set of physical processes for a given bright band.

2. Previous studies

The phenomenon of the radar bright band, due to the increase of reflectivity following the melt of ice particles falling just below the 0°C level, has been recognized since the early days of radar meteorology. Interpretation of the physical processes leading to the effect still presents a challenge in as far as the details of the physical processes are inadequately understood and depend on the input particle size and shape falling from above. As pointed out by Drummond et al. (1996) and papers quoted therein, the importance of changing refractive index for microwaves as melting proceeds is substantially offset by the increasing fall velocity and decreasing size following melting and is consistent with Doppler velocity measurements for a limited number of cases. The interpretation of cases departing from this simplicity is sought in terms of aggregation above the top of the 0°C level and aggregation, coalescence, and breakup in the melting region itself. Evidence for the presence of large aggregates in the melting region comes from aircraft measurements of particle images (Willis and Heymsfield 1989) and mountain measurements from a spectrometer embedded in the snowfall (Barthazy et al. 1998). Evidence of particle breakup is less definitive. Knight (1979) collected melt-layer particles in chilled hexane and demonstrated that water drops were skewered by a thin (some tens of micrometers in diameter) ice crystal and further found water drops preferentially located at crystal intersections and also covering hexagonal plates. Aircraft observations do show smaller particles as part of the distribution, but the melt rate is rapid for smaller particles and the actual occurrence of the breakup process is not readily observed in flight. Laboratory studies of Mitra et al. (1990) in the Mainz vertical cloud tunnel simulated freefall conditions of dendrite flakes collected in natural events and increased the air temperature to melt the crystals in order to simulate fall to a lower warmer level. The relative humidity was maintained near 90%. In association with lateral and helical motions, the melt products tended to move toward the center of the flake, lodging preferentially at branch intersections and collapsing at an advanced stage of the melt process. Ice particles were occasionally shed from the dry exterior, as were drops, although they may or may not have contained an ice component. A different approach was used by Oraltay and Hallett (1989) by growing ice crystals of differing habit from the vapor in a dynamic thermal diffusion chamber incorporated in a closed-circuit wind tunnel under independent control of temperature, supersaturation, and wind speed. Crystals grew into the wind direction and could be rotated and evaporated and/or melted under controlled temperature and relative humidity in reverse flow. It was found that thick columns and plates melted and evaporated without breakup. Thin columns, needles, and dendrite crystals, on the other hand, shed mixed ice and water fragments when the relative humidity lay below 80% over ice. Under these conditions melting droplets were localized along needles or dendrite arms that detached as further thinning occurred by evaporation and/or melting. An important aspect of the melt of ice particles under nonequilibrium conditions was pointed out by Matsuo and Sasyo (1981) in as far as high relative humidity at temperature above 0°C would lead to melting by condensation as well as by sensible heat transfer.

The present work extends the earlier studies to greater departures from equilibrium from the viewpoint of delineating more precisely the physical conditions under which such breakup occurs and whether drops not containing ice are shed. More extreme departures from equilibrium are simulated as larger mixed ice/water-containing particles falling to ambient temperatures as high as +5°C under near-saturation conditions [modeled by Szyrmer and Zawadzki (1999)] or as mixed-phase particles lofted to lower temperatures below 0°C in weak updrafts.

3. Experimental techniques

In order to simulate the various ice crystal processes in the laboratory, it is necessary to devise a system such that not only can ambient conditions be controlled and changed to give the desired crystal habit and size, but the time scale appropriate for the atmosphere of crystals falling toward and through the melting level must be reproduced. This is a formidable undertaking as not only do crystals have to be nucleated and grown, but also aggregated, evaporated, and/or melted under controlled conditions, ideally under free fall (Fig. 1). The experiments described below are a compromise in as far as crystals nucleate on a vertical 80-μm-diameter

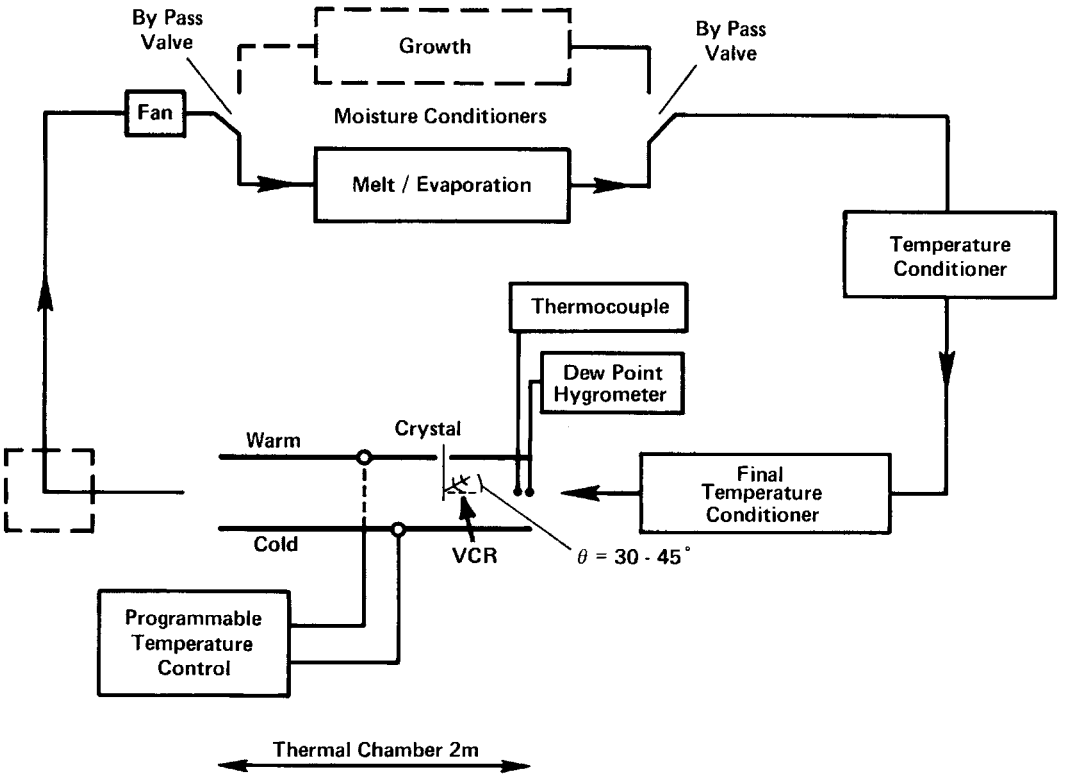

FIG. 1. Closed-circuit dynamic diffusion chamber for growth, melt, and evaporation of ice crystals. Crystals are grown at a selected temperature, supersaturation, and air speed on a vertical glass filament 80 μm in diameter (bottom left) at the end of the diffusion section having ice both top and bottom, with the top at a higher temperature. The sample is then rotated to face the flow (right) in the opposite direction at a controlled uniform temperature and frost/dewpoint of the conditioner and temperature controlled by the isothermal chamber. Non-steady-state situations are conveniently reproduced by increasing air velocity up to 0.5 m s^{-1} for vapor growth and up to 1.5 m s^{-1} for aggregate melting. Crystal behavior is videorecorded at 30 fps. Arrows show flow direction for evaporation or melt; airflow direction is reversed for growth.

glass filament, grow, and are otherwise manipulated in an environment at controlled supersaturation and temperature in air moving at an independently controlled velocity. Although this velocity is chosen to simulate and track the likely fall velocity of the particle of interest, the actual fall velocity of the melting particle must respond to the changed shape and the spatial distribution of the drops, and is not taken into account in these studies. The thermal effects of the filament have been demonstrated to be negligible in as far as rate processes are essentially unchanged for distances in excess of a few fiber diameters outward. The techniques used follow those described by Oraltay and Hallett (1989) emphasizing non-steady-state conditions. Further details of the chamber design and operation can be found in Keller and Hallett (1982).

4. Results

Investigations are described through visual sequences of the melt/evaporation of crystals at airspeeds of 10–50 cm s^{-1} for individual crystals and up to 150 cm s^{-1} for aggregates. Crystals are grown in the form of columns ($-4°$ to $-5°$C) and plates ($-12°$ to $-16°$C) at subwater saturation. Needles, including high supersaturation needles having an angle of 25° to the *c* axis, are grown at $-4°$C, with supersaturation from water saturation up to 50% over ice and airspeed to 20 cm s^{-1}. Dendrites with plate and rounded tips are grown at $-15°$C from water saturation to 20% water supersaturation with airspeed up to 50 cm s^{-1} to give different arm spacing.

a. Melting of ice needles and columns

The sequence in Fig. 2 shows needle and column crystals grown on 22° spikes at a temperature of $-4°$C and an ice equivalent supersaturation of greater than 34% depending on ventilation. Such growth might be produced by ice growth from the vapor dominated by the presence of partially frozen mixed-phase particles having a surface temperature near 0°C. The crystal *c* axis lies along the bisection of the "V" (Fig. 2a). With reversed flow at 20 cm s^{-1}, an air temperature (T_a) of $+2.8°$C, and a dewpoint of $+1.5°$C, melting begins (Fig.

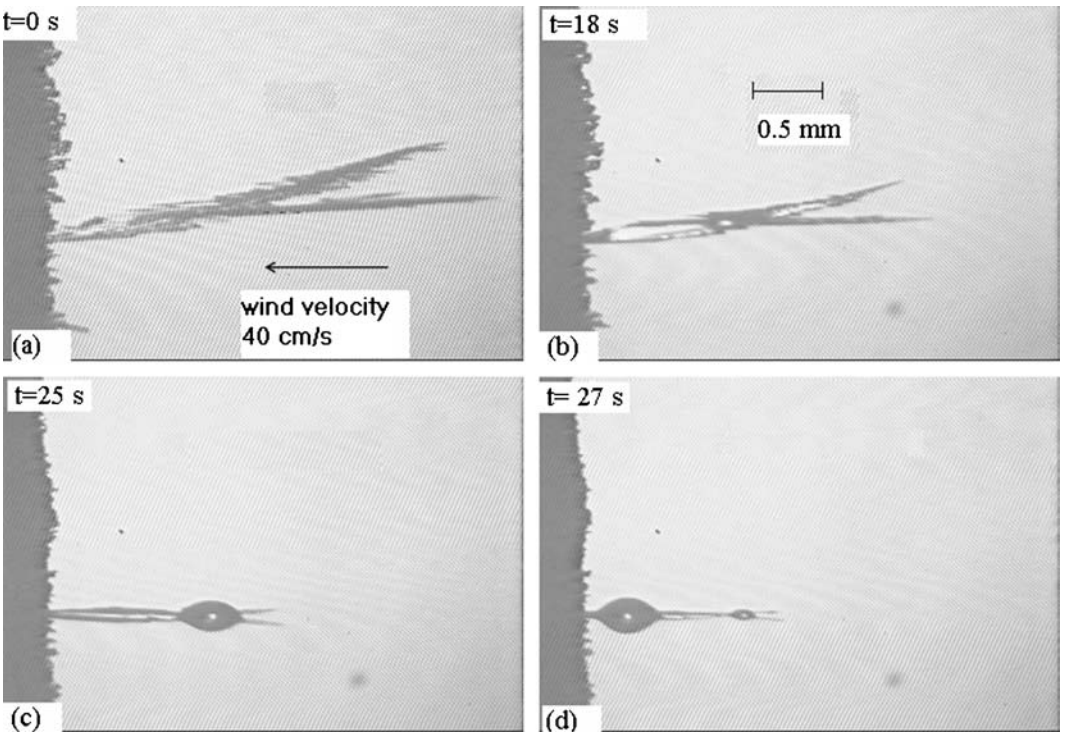

FIG. 2. Time evolution of columns grown along the *c* axis and ice spikes grown at 25° to the *c* axis near −4°C at water saturation and an airspeed of 20 cm s^{-1} that are exposed to an airstream originally saturated at +4°C and cooling on entry into the diffusion chamber to +2.8°C. (a)–(d) Liquid condenses on the ice columns, eventually residing preferentially at crystal intersections. Drops move with the airflow component along the crystals as they reach a diameter >200 μm. External contact angles range from 150° to 165°.

2b) and the liquid moves with the airflow to a location at the intersection of the spikes (Fig. 2c). With further melting, the drop grows and moves farther along the original column leaving a smaller drop, at the original intersection (Fig. 2d). The crystal tips are sharp and do not show the presence of liquid. As time evolves, liquid is apparent on the surfaces and away from the tips. By the moment shown in Fig. 2c the tips have significantly retracted and liquid can be seen only at the intersections of crystals. Drops show distinct internal (external) contact angles between about 30° and 15° (150° and 165°; Fig. 2d) and are retracting with the airflow direction. Drop contact angles are unchanged toward and away from the drop motion; qualitatively it is observed that they differ over some ±5°–10°, depending on the environmental saturation and whether the drop is growing or evaporating.

b. Melting of dendrites

Figures 3–7 show different shapes of melting dendrites under different environmental conditions. The distribution of water drops resulting from this melting is shown on ice filaments (produced by the dendrite melting) and also distributed on the remaining faceted regions of the dendrite basal plane on flat surfaces of the dendrites lying along the crystallographic *a* axes before they have melted to filaments, with the liquid confined away from the edges because of surface tension effects.

Figure 3 shows melting of a dendrite grown at −15°C to give a different crystal orientation (dendrite branch, *a* axis) compared with Fig. 2 (needle, *c* axis). It has been reoriented to face the wind coming from the direction away from the support. As melting proceeds [T_a and wet-bulb temperature (T_w) > 0°C], liquid spreads downwind along the central flat axis of the dendrite and also along the side arms (Figs. 3a–c) and the upstream crystal melts and reorients (Fig. 3d). Both air temperature and ice-bulb temperatures (T_i) are now reduced (Figs. 3e–g) with $T_i = -2$°C. The drop now begins to freeze as can be seen from the small protuberances (Fig. 3h). The drops make finite contact angles with a central ice filament, about 120° external, increasing as the temperature drops and freezing begins.

Figure 4 shows drops resulting from arm melt running along dendrite arms and branches (the central axis) along the airflow. Liquid is retained at the larger dendrite tips on the lower crystal, shielded from the airflow, whereas in the upper crystal (exposed to the airflow) drops locate along the melting dendrite axis (Fig. 4b) and move downstream along the crystal (Fig. 4c). This crystal eventually breaks off (Fig. 4d) carrying both the central ice filament and the drop together.

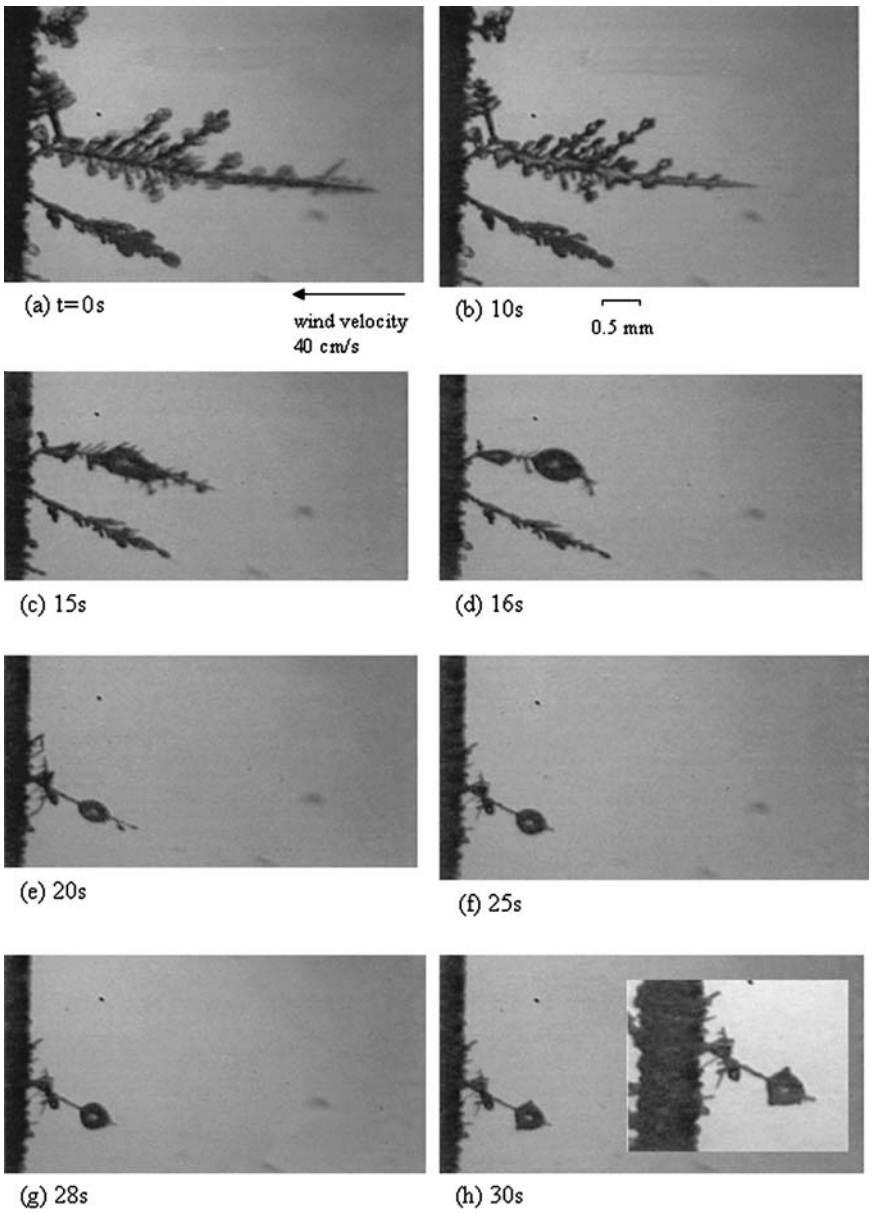

FIG. 3. (a)–(d) Evolution of a drop centrally located on a thin ice filament having been produced by melting of dendrites at temperature $T_w > 0°C$. Note the presence of liquid on the dendrite surface in (b). (e) The crystal is suddenly introduced to an evaporating environment with $T_i < 0°C$. (f) The drop is cooling but has not had sufficient time to freeze. (g), (h) It begins and concludes freezing and loses its smooth shape [(h) insert]. It has been located at a point following the initial melting and subsequent freezing of the ice away from the drop, which prevents it from wetting the column ice surface. The crystals are oriented into the wind maintained at about 40 cm s^{-1}. The drop maintains a well-defined interface angle with the ice (external angle approximately 120°). It eventually freezes with the same orientation as the ice column, as shown by the side protuberances in (h).

Figure 5 shows similar events with dendrites grown under much higher supersaturation than those in Fig. 4 and having finer side arms. The dendrites melted but rarely broke up under these conditions, liquid being removed from the neighboring ice surface to larger drops by capillary forces. These figures show clearly that liquid covers the ice surface until the radial dimension has shrunk to about 50–100 μm, below which the capillary forces appear to dominate (Figs. 4d and 5d). The drop begins to form symmetrically around the ice, as a drop on a filament, approximating the form of Fig. 3. This observation is consistent with minimized

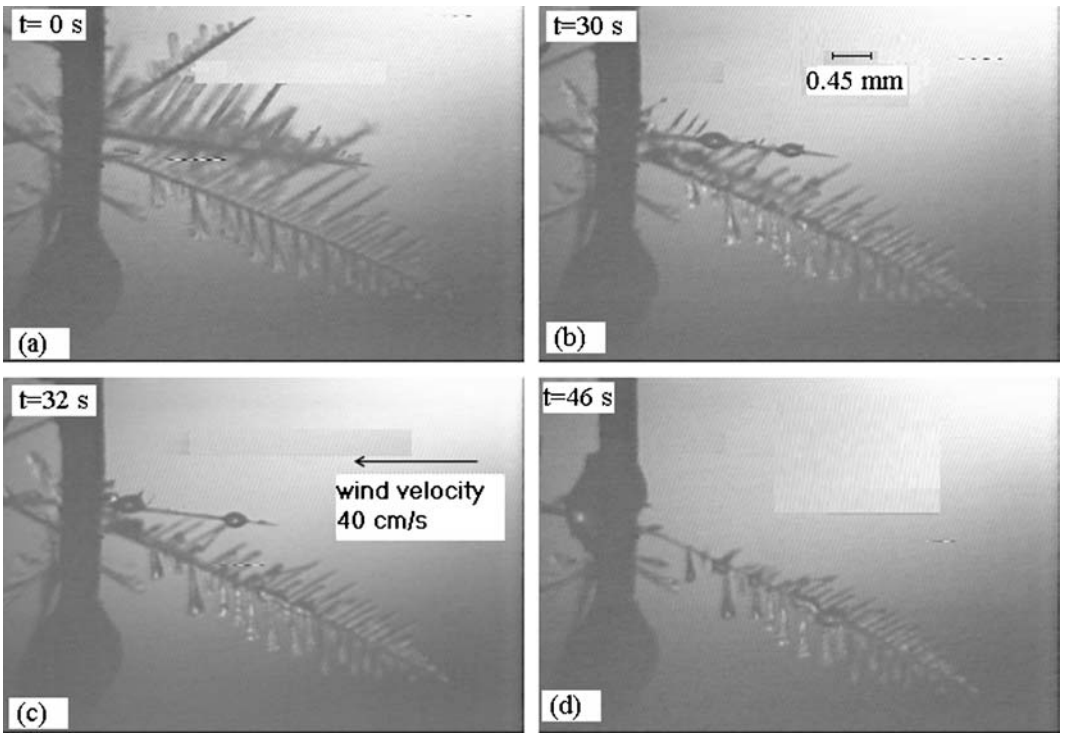

FIG. 4. (a), (b) Water condensing on an ice crystal formed by melting of a dendrite under high water saturation under similar conditions to those in Fig. 3 but leading (c), (d) to discrete drops. The neighboring dendrite below is melting, and the liquid runs along each side arm to a location at the flat surfaces of the tip. Breakup of the upper long thin crystal eventually occurs close to the support, which locally is a source of heat as compared with the crystals themselves. None of the dendrite arms or branches broke away in this sequence. The upper long thin crystal shows the drops growing by condensation and melting; they move in the wind direction when they have reached sufficient size.

surface energies under different environmental conditions.

Figure 6 shows multiple effects depending on whether the melt water was located on the tips or main arms or branches of the dendrite. The effects of liquid movement by capillary forces are clearly shown in Fig. 6c, leaving very thin liquid-free ice filaments near the tips; the liquid being incorporated into the nearby drop to the left. The crystals at the extreme tip are subsequently broken off as shown in Fig. 6d.

Figure 7a shows a dendrite growing at −15°C as the wind speed is increased from 10 to 40 cm s^{-1}, resulting in a highly branched dendrite toward its end. This sequence is then melted in air at +0.8°C (Figs. 7b–c). As melting progresses, wider arms are covered with a water layer (Fig. 7b) but narrower tips appear to be water free and evaporate (Fig. 7c). Breakup of continuous water coverage beginning in (Fig. 7c) becomes more evident in (Fig. 7d) as the ice filament thins. This filament is thinning continually, but shows no sign of melting and appears to be evaporating indirectly despite the known condition of water supersaturation and the growth of drops. No water layer is apparent, but one could be present as a layer not visible at this resolution. This argument is also applicable to other ice regions between drops on filaments. Eventually, the ice breaks (Fig. 7d), leading to the release of an ice-containing drop. The ice support had thinned from 100 μm to below 20 μm before breaking, despite being subject to aerodynamic forces and its own weight. Here also it is inferred that drops formed at discrete intervals, and having finite contact angles on ice filaments, *a* or *c* axis, are apparently separated by nonwetted ice, suggesting that the ice temperature, necessarily below 0°C, is maintained below ambient, and is evaporating by heat conducted from the growing drops themselves. The process may still be giving transport of water substance as a thin layer from the ice surface to the liquid drop; also the presence of trace impurities cannot be excluded. Visible condensation is *not* occurring because of the thermodynamic inability to nucleate and condense a thicker liquid film on the ice surface (see section 6).

c. Melting plates

Figure 8 shows the same phenomena for plates that were grown on the ends of dendrites by reducing the air velocity to near zero prior to initiating melting. The evaporating tip of the plate appears to be dry in the sense that water-covered ice gave the shiny appearance

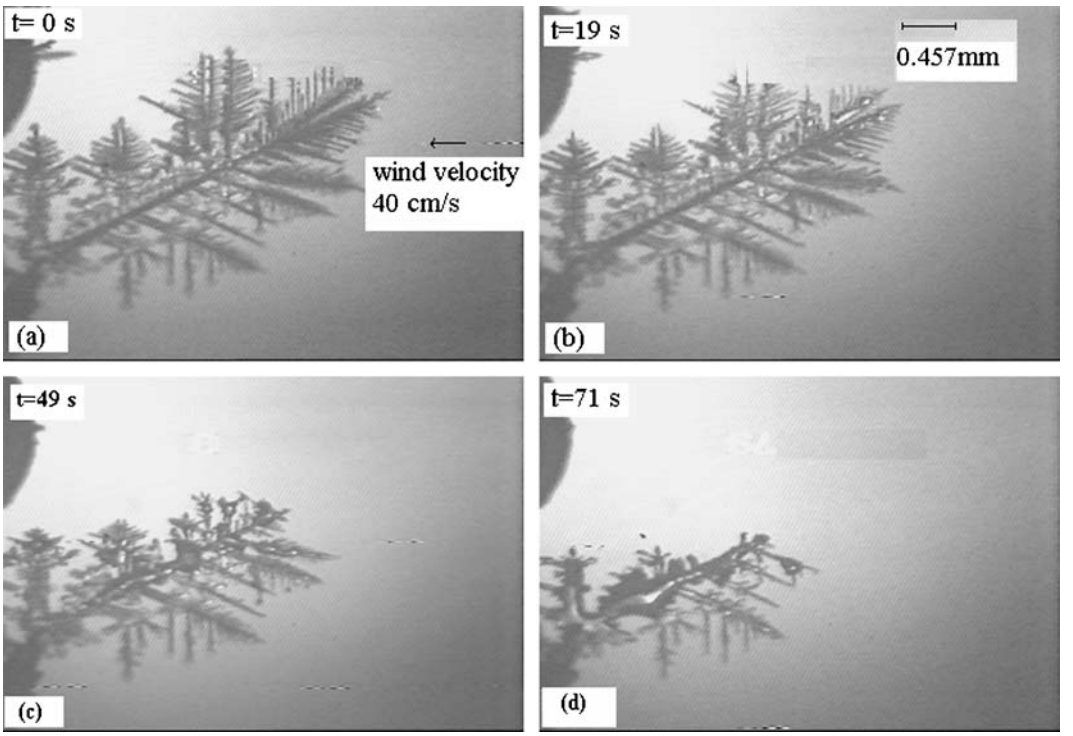

FIG. 5. (a)–(d) Sequential movement of water drops and coalescence along the wind component on an array of dendrites with arms at close intervals grown under higher ice supersaturation (50%) and a wind speed of 40 cm s^{-1}. Breakup does not occur under these conditions. (b) The water moves back along the wind direction covering the flat dendrite surface, (c), (d) eventually beginning to form larger drops.

as in Fig. 8b and could be seen to be moving around prior to being retracted from the surface. The narrow tips seen in (Fig. 8c) break off in the airflow at a thickness of about 20 μm.

d. Aerodynamic molding

Breakup and aerodynamic molding are shown in Fig. 9. Here dendrites, having grown into the wind, were melted and evaporated in reverse flow, and subsequently deformed by being wrapped around the support and then rotated a second time to face into the flow, whereupon further melting and breakup occurred. Idealized shapes of these melting patterns are shown later (Fig. 11).

5. Physical processes: Heat and vapor transport

The detail of the behavior of individual particles is now seen to be more complicated in as far as we must deal with gradients of properties *across* the particle as well as differences *between* particles. For example, Figs. 2 and 3 show a drop in an apparently stable configuration centrally located on a thin ice filament, either the *c* or *a* axis, respectively. The conditions for this situation are that both the drop and the ice particle are evaporating, with the temperature of the ice below 0°C; otherwise, the droplet would be on the move and wetting the ice. The water on the other hand is clearly in contact with the ice, but could be below 0°C at the outside and must be close to 0°C near the ice–water interface, otherwise ice growth would be taking place into the droplet. Under the conditions of this particular experiment, it is possible to define wet-bulb and ice-bulb temperatures showing that if there were complete isolation of the drop, a growth velocity of the ice of $V = 0.1T^2$ cm s^{-1} (T = drop supercooling) would allow ice to penetrate to the surface of the liquid. For T = 1°C the growth velocity is 1 mm s^{-1}, and so clearly the supercooling must be considerably less than this for the drops to persist unfrozen. We might expect some cooling of the drop surface, remote from the ice, leading to very slow growth of the ice *inside* the liquid, but at a velocity well below a few micrometers per second. This is evident should the drop eventually be blown away as a slight thickening of the ice column as described by Knight (1979). With the drop at a temperature above 0°C, as could occur during growth with a dewpoint above 0°C, not only will melting of the ice take place both inside and outside of the drop, but water will tend to run along the ice to be localized at ice cross points in a snowflake. The relationship of these processes to particle breakup is critical because ice thinning may occur either by ice evaporation driven by an ice undersatura-

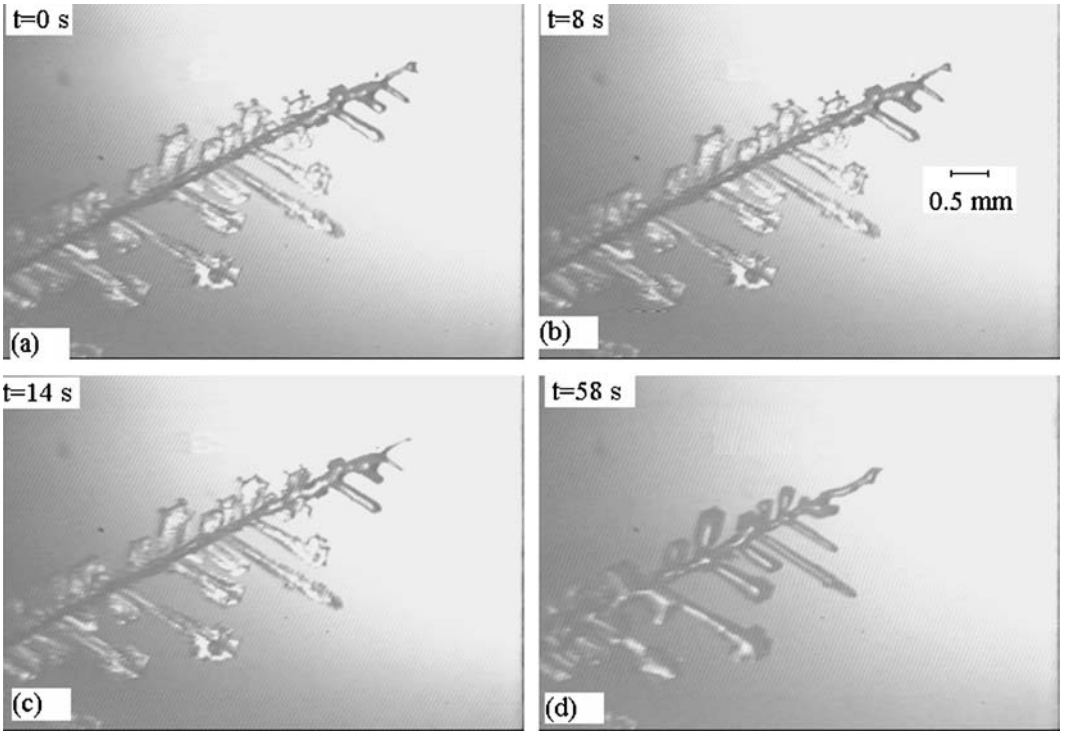

FIG. 6. (a)–(d) Dendrite crystals grown near −15°C at water saturation at 20 cm s^{-1}, with the air speed subjected to air saturated at +3.7°C. The airspeed is slowly increasing from 10 to 20 cm s^{-1}. As melting progresses, the drop perched on the disappearing dendrite follows the airflow and (c) moves to the original crystal followed by the loss of the ice extremity.

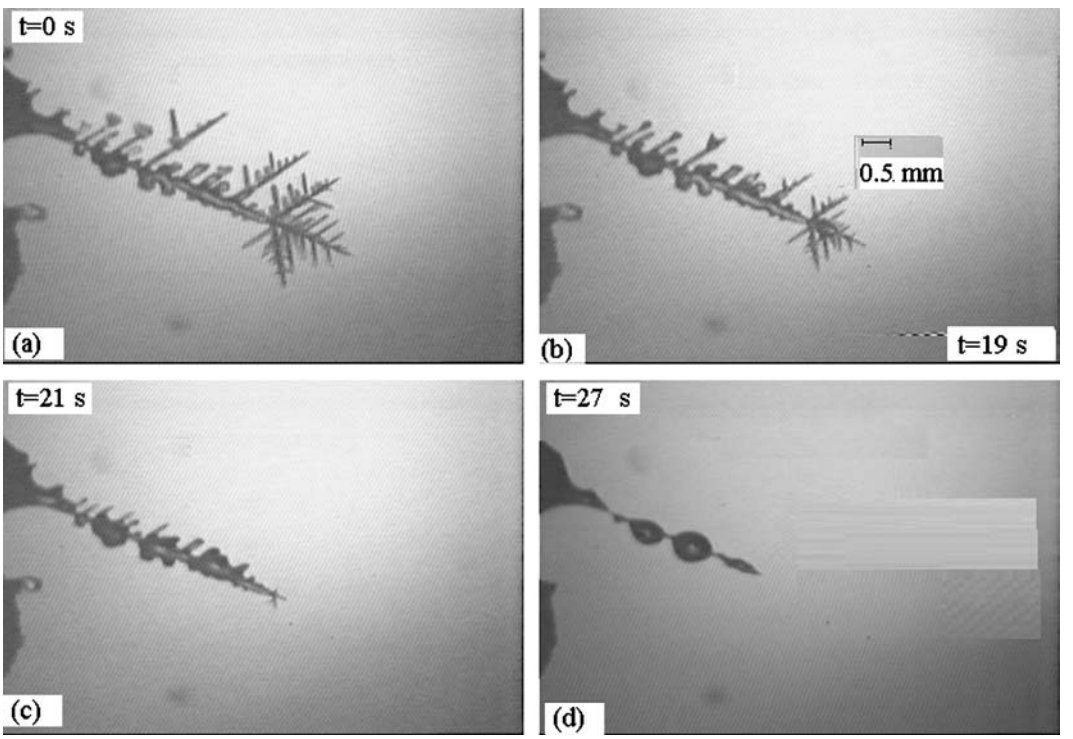

FIG. 7. (a)–(d) Melt sequence of a dendrite with narrow branches and arms leading to continual surface coverage on the basal plain, which subsequently breaks up into individual drops as thinning occurs (see text).

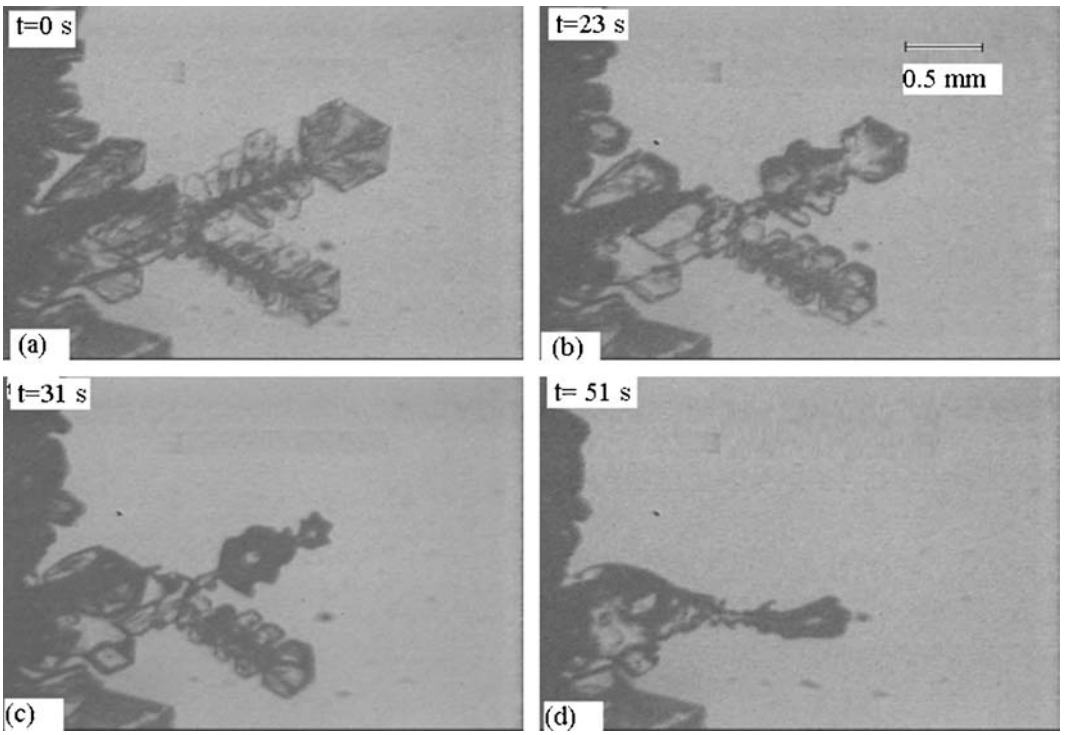

FIG. 8. (a)–(d) Melting of plate crystals, size 300 μm, by condensation over a flat area, with a temperature of +2.1°C. The liquid fails to break up into drops (as occurs for a column or dendrite) but (b) follows the ribs of the plate (end plates). The liquid is present as a sheet, some tens of micrometers thick near the plate center. Such crystals have not been observed to shed drops or to break up although a complete arm may bend or break off as in Fig. 11.

tion or by water layers forming localized drops having a temperature above 0°C by condensation (away from the ice itself) from an environment saturated at a temperature above 0°C. These considerations point to the importance of specifying the ambient conditions in terms of a dewpoint, T_d, or a frost point, T_f, determined by some average local hydrometeor condition and a local wet-bulb temperature, T_w, and a local ice-bulb temperature, T_i, determined by the geometrical structure of the hydrometeor itself and having a range of values over the surface. In the latter case, all we can do is provide limits or values in the neighborhood of water or ice protuberances. It is to be remembered that the wet-bulb temperature is *greater* than the air temperature for a specified supersaturation (assuming no condensation takes place on local cloud condensation nuclei), as is the frost point temperature. It is convenient to specify these processes on a vapor density–temperature plot with reference to the saturation curves with respect to water and ice (see Fig. 10).

We follow previous investigators, using a first approximation equating the growth rate equations for heat and mass:

$$dq/dt = 4\pi K F_h C(T_s - T_e) \quad \text{and} \tag{1}$$

$$Ldm/dt = L4\pi D F_m C(\rho_s - \rho_e), \tag{2}$$

where L is the appropriate latent heat of vaporization; s is the surface conditions; e is the environmental conditions; C is a geometrical factor; F_m and F_h are the ventilation effects for mass and heat, assumed equal to sufficient accuracy; and K and D are the air thermal conductivity and water vapor diffusivity in air, respectively.

In equilibrium

$$dq/dt = Ldm/dt \text{ or } T_s - T_e = -LD/K(\rho_e - \rho_s). \tag{3}$$

Again, to sufficient accuracy, the slope of the line, $-LD/K$, may be assumed constant for a given pressure although in reality there is a slight temperature dependency of the latent heat of water and ice for different processes. Convenient representations of Eq. (1) are straight lines of slope $-LD/K$ intercepting the T–ρ saturation curve for water and ice from the selected environmental points: T_e and ρ_e. The diffusion coefficient is inversely related to pressure, which cannot be ignored; the slopes for pressures of 1000 and 500 mb (hPa) are indicated in Fig. 10.

6. Physical processes: Capillary effects

We distinguish the following situations that may arise as ice particles enter different environmental condi-

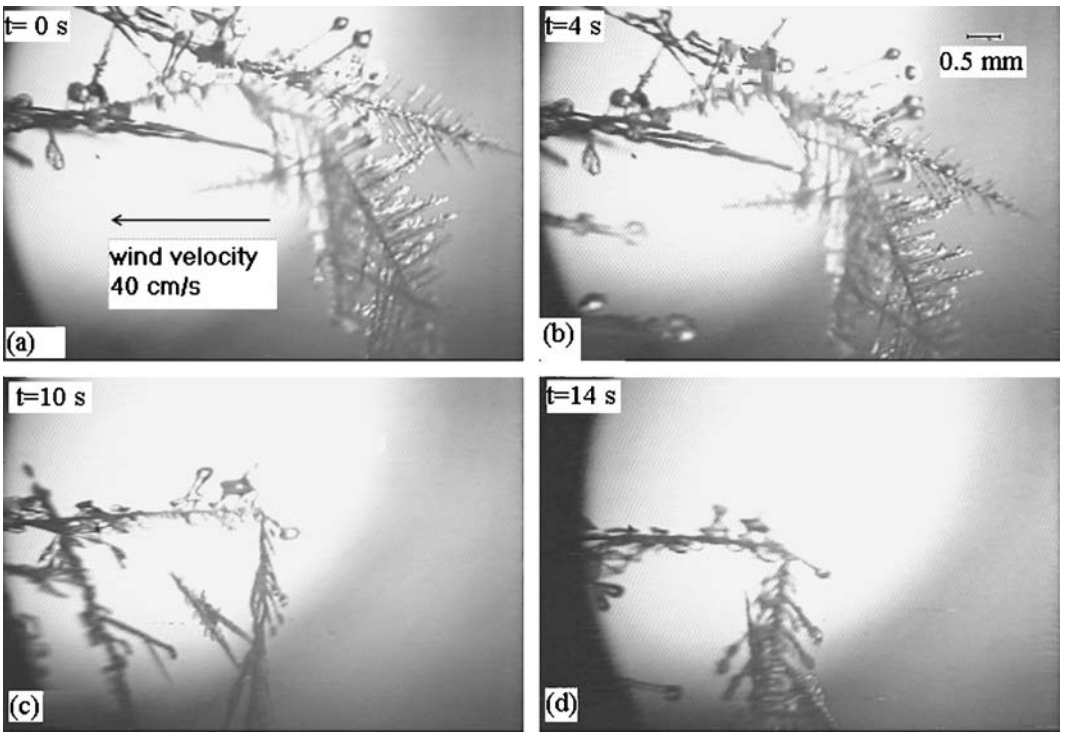

FIG. 9. (a)–(d) A complex sequence of dendrite crystal growth (−15°C, 30 cm s^{-1}), melt, and evaporation. Growth occurs first as dendrites into the wind at −15°C, water saturation, and 30 cm s^{-1} wind speed. The wind speed lowers to 10 cm s^{-1} giving plates toward the −14°C level and is then returned to the higher velocity. The crystals are then rotated so that the wind direction is reversed. Air temperature is +3.7°C, cooling to +0.8°C upon approaching the crystal. Crystals (b) melt and break up; (c) some detach, while (d) others undergo an aerodynamic molding, moving downwind.

tions: ambient dewpoint $T_d > 0$°C; $T_w >, = 0$°C. Water will condense on any hydrometeor containing ice, locking its temperature to 0°C or a little above, depending on the temperature gradients in the overlying water (see discussion in Johnson and Hallett 1968). Ice will be melting at a rate depending on the sensible and latent heat fluxes from the environment and will wet all exposed ice surfaces. There is an important caveat here. The process of drop coalescence involves growth of a larger drop by absorbing a smaller drop or alternatively absorbing a shallow cylindrical water layer on the surrounding ice filament. Thus, in view of the internal pressure differences, two cases arise: First, for two drops

$$\Delta P = \sigma(2/r_1 - 2/r_2), \tag{4}$$

where σ = surface tension and 2 comes from the equal radius curvature in two directions at 90° for a spherical surface. The smaller drop, r_2, has higher capillary pressure and is therefore incorporated into the larger drop, r_1. Second, in the case of a drop interacting with a uniformly water-covered cylinder radius r_3, the water cylinder excess pressure compared with a spherical drop radius r_2 is

$$\Delta P = \sigma(2/r_2 - 1/r_3) \tag{5}$$

and gives the criterion for whether a shorter cylinder remains stable or a longer cylinder breaks up into discrete drops. A long, thin-walled water cylinder, such as a melting needle, is highly unstable with respect to itself and in the event of contact with any nearby large drop. The net result is in agreement with the observation that the coalescence of drops and disappearance of water cylinders is readily seen to occur. This happens for drops on ice filaments resulting from melting needles (Fig. 2) and also from drops resulting from melting dendrites when they are sufficiently thin (Figs. 3, 4, and 7), as well as the individual drops on ice filaments. The time for coalescence is short, to be approximated by the drop oscillation frequency, and is approximately 0.01 s for the sizes considered here. Drops are stable on large flat surfaces (as in Figs. 5, 6, and 8) provided that the drops are isolated at the crystal edges through surface tension effects and they have a large contact angle. It may be expected however that for very large flat ice surfaces, individual drops could exist as in the case of ice needles. As discussed previously, on the submicroscopic scale, melt water may be present on the ice, but is so rapidly transported to neighboring larger drops that it does not become visible.

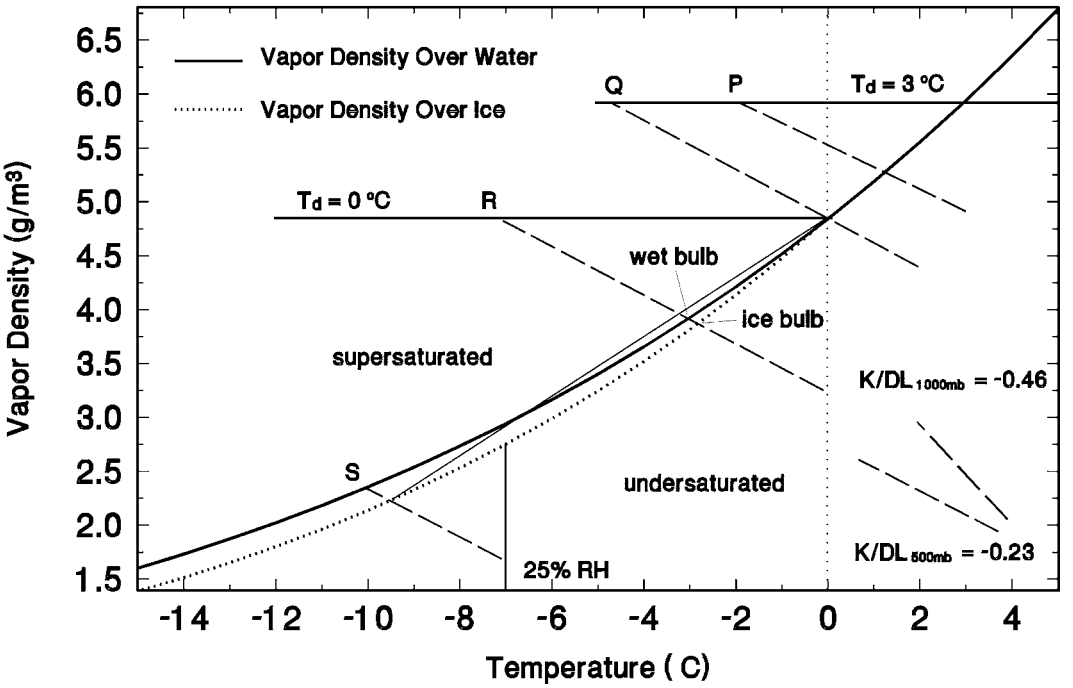

FIG. 10. Schematic showing different conditions with respect to the saturation vapor density over water and ice of particles maintained at selected environmental conditions of undersaturation and supersaturation. (bottom right) The different slopes, $-K/DL$, [Eq. (3)] depend upon the ambient air pressures: 1000 and 500 mb (hPa). The horizontal line through +3°C on the saturation curve P ($T_d = +3$°C) represents an environment in equilibrium with both drops and saturated air at this temperature. An idealization (no droplet condensation) of isobaric cooling of saturated air leads to supersaturation and a wet-bulb temperature above ambient given by the dashed line through P at the intersection of the vapor pressure curve. (This point also represents the conventional wet-bulb temperature of a drop in air evaporating into an undersaturated environment from any temperature to the right of the saturation curve on the dashed line.) The horizontal line representing continued isobaric cooling through $T_w = T_i = T_d = 0$°C to the point R gives supersaturation and a supercooled wet-bulb temperature (−3.1°C) and an ice-bulb temperature of −2.9°C (T_w is a lower temperature than T_i). The diffusion of water vapor and heat in air saturated at 0°C to ice at −9.5°C (representing a drop in the process of freezing on a cold ice particle) over ice is represented by the straight line joining the two points and is supersaturated above the supercooled water vapor density curve; cloud droplets could nucleate on any CCN present; see text. In another scenario point S at 25% relative humidity over ice (frost point = −12.6°C) gives an ice-bulb temperature at −9.5°C at the intersection of the dashed line with the ice curve and the supercooled wet-bulb temperature at a lower temperature at points, (−10.1°C). This diagram readily shows, for both supersaturated and undersaturated conditions, the temperature differences of various processes by the selection of the beginning environmental conditions and drawing the appropriate $-K/DL$ line to the ice or water vapor density curve. Further uncertainties arise for non-steady-state conditions, as particles are cooled or heated by changing evaporation/condensation processes and temperature gradients are present within the particles.

Thus any water appearing on an ice filament as a cylinder skewering a drop (as in Figs. 2 and 3) is rapidly removed and has difficulty reestablishing itself in as far as nucleation of a uniform cylinder coat is an unlikely process as the energy involved is large from a fluctuation consideration. So, it does not happen, and the cylinder remains dry in spite of the high supersaturation of the environment (say, water saturation at +3°C compared with water saturation at 0°C, a saturation ratio near 20%). It is emphasized that the observations do not preclude a flow of a thin layer of water from the ice to the drop, which may not be readily visible.

A further complication arises in as far as drops on a filament that is wetted are subject to instabilities as shown by Carroll (1976). An aspect of the physics herein may be related to the drop separation shown in Figs. 2 and 3. The contact angle is clearly nonzero and appears related to the evaporation and growth of both water and ice. It is apparent that the contact angle measurement is subject to uncertainty because of the viewing geometry, and some spikes may appear to have a 90° contact angle (Fig. 11f) as they are hidden behind the drop. Most contact angles (in the liquid) lie between 37° and 80° (143° and 100° in air; Fig. 11), depending on the conditions. The contact angle is therefore to be interpreted in terms of differences of surface energies depending on local temperature and growth/evaporation rates and the shape and diameter of the ice filament. This is a highly complex situation, requiring further investigation; it has the potential to give insight

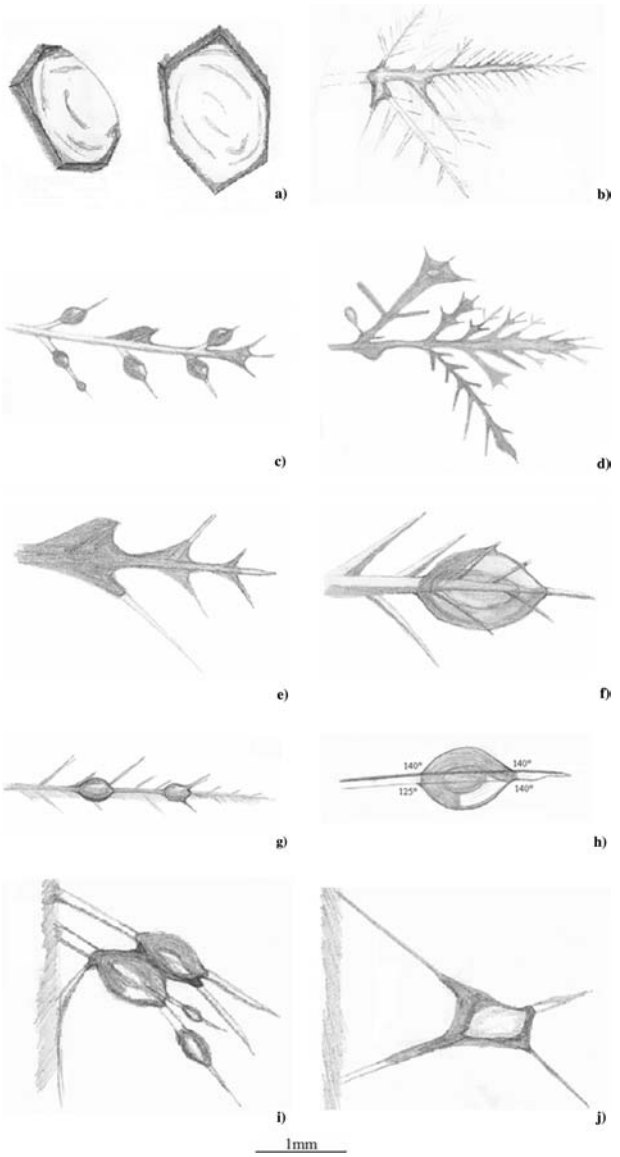

FIG. 11. Idealized forms of melting resulting from the condensation of vapor on the ice as a liquid or direct melting in an environment at higher temperature or both. Scale of 1.0 mm is shown at bottom. (a) Melting of extended basal or prism planes results in near-uniform water layers covering each plane. (b) Similar effects occur on the flat regions of dendrites. (c) Separated drops form as dendrite branches melt to ice filaments and settle along each branch or at the central arm branch junctions. (d), (e) At higher relative humidity (>80%) drops are segregated at branch-arm intersections, the location being influenced by the airflow during fall. (f), (g) Larger independent drops reside across several branches on each dendrite arm branch. (h) Each drop makes a contact angle with its ice filament whose value depends on evaporation rate (less) or growth rate (more). Measurements of angles are difficult (±5°) for reasons of both perspective and shielding and are best made in air as shown, giving contact angles (in liquid) of 40° and 55° (in air of 140° and 125°) in this case. (i) Drops are located at intersections of high supersaturation 22° ice spikes with side columns. (j) Drops are also readily located at crystal intersections in all aggregates leading to a drop array with a regularity of spacing. Sketches from video images courtesy of G. Vidaurre.

into the structure of liquidlike layers on ice as influenced by the ambient relative humidity. It is doubtless impurity dependent.

With an ambient frost point below equilibrium at the temperature of the environment, ice and water will be evaporating; any remaining water will not wet surrounding ice. There is a distinct contact angle of the drop on the ice filament, clearly visible in Figures 3 and 7, of some 37°–80°. Clearly conditions depart from equilibrium near 0°C although there are reasons for expecting that the drop will wet the surface at 0°C, as argued by Knight (1979). The long-argued issue of the nature of the ice surface near the melting point could be subject to resolution with more precise measurement of the contact angle of a water drop on ice under a high degree of temperature and relative humidity control and the exclusion of impurity.

Under nonequilibrium conditions, for either growth or evaporation, the temperature differences may well occur between a liquid and a solid leading to growth or melt at the three-phase, ice–water-vapor interface such that the observed finite contact angle exists. With water supersaturation in the environment, both ice and water will be growing, the temperature of the water will be >0°C, the ice will be close to 0°C, and there will be lateral gradients of both temperature and surface properties. Eventually wetting must occur as the interface temperature rises toward equilibrium. In the case of water supersaturation below 0°C (equilibrium), the temperature of the drop may be below 0°C but above the ice temperature as latent heat is released; the ice temperature itself may be above ambient but not above 0°C. Thus the ice will be growing at the three-phase interface and the finite contact angle may persist. The situation of the water being above 0°C, the ice below 0°C, and both growing from the vapor cannot be excluded. With undersaturated conditions, both ice and water may be evaporating, with the ice submerged in the water and growing as a transient.

Let us consider the ice-bulb temperature approaching 0°C from a water-saturated or supersaturated environment. Wetting may occur at a temperature a little below 0°C if a liquidlike layer exists (Furukawa et al. 1987); this could itself be supersaturation dependent. This situation could also occur in the case of trace-soluble impurity. This process would occur for an extensive near-flat surface (Figs. 11a,b) and less likely for a thin ice needle (see also Fig. 11h).

The implication for a radar return is a distributed or central target depending on the vertical profile of T_w near 0°C rather than T_a itself. An alternative scenario is where water from the melting outer regions of a particle fails to penetrate, at least initially, to the lower-density, colder, inner regions. Under these conditions, the approximation of a partly spherical shell of water on an ice–air matrix may be a possible approximation to model.

7. Application to the atmosphere

Cloud situations far from thermodynamic equilibrium are used to demonstrate the existence of highly supercooled drops separated by air at various distances from ice particles and ice nuclei; that is, the conventional ice crystal precipitation process. Here we emphasize a different aspect of nonequilibrium where both liquid and solid phases are present as a melting or freezing ice–water mix, influencing or being influenced by a neighboring but separated drop or ice particle. The more complicated case occurs when different regions of the same particle expose areas of different phase, as the growth of rime, or the melting and redistribution of the water over the ice by surface tension as in the present case. The ice–water mixed-phase particle, as a freezing or melting drop, leads to an important simplification: the temperature of the mix departs only marginally (a degree or less) from the equilibrium melting–freezing point, because the ice–water thermal conductivity is substantially above that of the surrounding air. This simplification has important implications in that both vapor pressure and temperature are substantially constant and close to 0°C. Neighboring particles are subject to these boundary conditions; thus there are implications for the thermal radiance and satellite signature of these particles (Black et al. 2003). Equation (3) implies that the regions between a mixed-phase particle and a neighboring particle may be specified by a line from 0°C to the ambient condition, as, for example, 0°C to ice −9.5°C (Fig. 10). Such a line may lie above and intersect the supercooled water curve, and give local water supersaturation, −6° to 0°C, with a maximum at −3°C of about 7% over water in this case, and local cloud condensation nuclei (CCN) may be activated to form cloud droplets.

The following situations arise:

(a) The falling of melting particles through air $T > 0$°C leads to a melt time approximately related to the diameter squared and the density. As particles fall to levels at higher temperatures, only the largest particles survive as an ice–water mix. These are influenced by their smaller neighbors, already completely melted and having reached a higher temperature, by as much as 5°C (Fig. 10). The region responsible for the radar bright band maximum optimizes wavelength-dependent scattering, combining effects of composition and the spatial distribution of melt water as described herein, together with size, fall velocity, and, hence, concentration. The location of the maximum depends on the details of the particle spectrum and these melt characteristics, with implications for the descent rate of the melting layer for regions of higher rates of precipitation (Mittermaier and Illingworth 2003). This situation of a few large aggregates, surrounded by a multitude of smaller drops at higher temperature, is still subject to the particle thermal lag as the aggregates fall to a warmer environment (Kamburova and Ludlam 1966). This would give a lower ambient relative humidity dependent on drop size, and could have an effect on larger drops and much larger aggregates. Such situations require high-resolution particle imaging to demonstrate these processes in sufficient detail for realistic modeling.

(b) The lofting in weak (<1 m s^{-1}) updrafts, associated with the melting level of smaller, previously shed, mixed-phase particles, to regions with temperatures below 0°C leads to their beginning to refreeze but maintaining a temperature close to 0°C. This can happen in an environment down to at least −5°C and can influence the growth of any neighboring ice particles at supersaturation well in excess of water saturation (50% as compared with 5% over ice at −5°C).

(c) The more complex situation is of a mixed particle with water and ice clearly separated on the same particle as the drop on an ice needle as shown in Fig. 2. The differences in temperature may be estimated from Fig. 10. Horizontal lines represent isobaric cooling of moist air without phase change, or serve as the boundary condition for diffusion growth. This air cools along the top line saturated at +3°C to points P (−2°C) and Q (−4°C). Consider a temperature difference resulting from growth (or evaporation) as given by the heat–mass transfer equations [Eqs. (1) and (2)], so that lines of slope K/LD represent temperature differences from any two points, with supersaturated regions to the left and undersaturated regions to the right of the vapor density curves. Thus the line through point R from undersaturation gives the ice-bulb and wet-bulb depressions from any point on the line at the intersections as temperature decreases; from supersaturation, the intersection points represent the increase in temperature from the release of the deposition latent heat by water or ice. Consideration of the deposition from the mixed particle at 0°C in intermediate regions to an environmental ice crystal at −9.5°C is represented by the straight line from this point to the equilibrium ice vapor pressure at this temperature; it is above the water saturation near −5°C. All situations are represented on the diagonal line through R.

For example, for air saturated at 0°C and an ambient temperature of −7°C, as with vapor produced by regions of lofted, freezing wet snow, the local temperatures are −3°C for water and −2.75°C for ice. Further the ice must be growing into the water, clearly an unstable situation. In reality, the environment would be saturated at lower temperatures, particularly from nearly completely solidified hydrometeors having lower temperature excess or lower environmental temperatures, which will shift the line from the vapor source to the sink below the water saturation. A further complex situation in-

volves the ambient water temperature slightly above 0°C and the water from the melting ice needle being drawn by capillary action into the drop, leaving the ice apparently dry (line through Q). Figure 10 further shows that temperature differences between growth (ice) and evaporation (water) at separate regions of the same particle may be expected to be not more than a few tenths of a degree (line through R to the intersections).

8. Conclusions

Snow crystal aggregates of different habits, melted under a range of environmental conditions, have shown a wide range of behaviors, from faceted ice crystals covered with melt water to aggregates carrying a distributed array of individual drops, with superficial similarity to dew drops on a spider's web. An important conclusion is that drop shedding with embedded ice occurs; such droplets could not supercool but would freeze as near-spherical single crystals and provide a mechanism for secondary ice production as an addition to rime splintering and the ice breakup by evaporation alone (Dong et al. 1994). Conversely, the shedding of drops not containing ice could give rise to regions of supercooled drops having significance for the specification of aircraft icing conditions. These microphysical processes depend critically on the regions where ice is growing from the vapor, particularly near −4° and −15°C, the region for ice needles and dendrites and their subsequent aggregation and fall through the region between −5° and +5°C.

A complete evaluation of the melting layer structure, leading to diagnostics for the radar bright band and the depth of the overlying isothermal layer, requires measurement of particle size distribution together with thermodynamic quantities on the same scale as the particle size distribution change with location. This poses a challenge for existing instrumentation since the large particles primarily responsible for the radar signal are sparse and the measurement statistics wanting. It is highly unlikely that simplistic parameterizations will be helpful here, and other strategies for prediction may be required. Comparison of the physical form of the particles, particularly the distribution of liquid and ice in individual particles, needs to be related to the level of interest; high-resolution aircraft imaging is required. In any case, the prediction of the vertical structure and evolution of the melting level, its descent with increasing precipitation rate, and inferences from the radar brightband reflectivity structure, although subject to specific constraints, remain open to interpretation. The absence of the bright band at shorter wavelengths may now be interpreted in terms of ice structure. It also is evident that coherent scattering of distributed drops over the aggregate can produce an effect that could influence the radar return as Bragg scattering (as a crystal lattice), more so at millimeter wavelengths.

Application of these ideas lies in precipitation falling from the moisture lofting in the sloping "conveyer belt" of a warm front. The structure of aggregates would be expected to change with temperature from dendrite to column as the front passes a given location and the temperature of the moist region aloft rises; different melting of resulting aggregates must dramatically influence the brightband detail and the decent rate of the isothermal layer as the warm front approaches. Bright bands formed in stratiform regions seeded by cirrus falling from aloft, as in hurricane outer regions or other large convective systems, would be much more likely to be influenced by riming, and this situation requires a separate study, as do more stable regions, potentially decoupled as discussed by Stewart et al. (1984).

The fallout of ice aggregates to the melting level, the changing depth of any isothermal layer, and the capability of forming or not forming a radar bright band depending on radar wavelength all need to take account of the particle habit and melting evolution described herein. Further exploration is required to determine the utility of any unique interpretation of the melting-level structure. Last, the nature of the ice–vapor interface and its detailed specification between localized drops skewered by an ice crystal poses a different, more fundamental set of questions for future investigation.

Acknowledgments. Support for John Hallett was provided by Grant ATMS 0224865 of the Physical Meteorology Program, National Science Foundation, Arlington, Virginia, and for R. G. Oraltay by a NATO collaborative grant (CRG 950770). Travel was supported through TUBITAK via UNISTAR, a United Nations program for international exchange.

REFERENCES

Bailey, M., and J. Hallett, 2002: Nucleation effects on the habit of vapour grown ice crystals from −18 to −42°C. *Quart. J. Roy. Meteor. Soc.,* **128,** 1461–1483.

Barthazy, E., W. Henrich, and A. Waldwogel, 1998: Size distributions of hydrometeors through the melting layer. *Atmos. Res.,* **47–48,** 193–208.

Black, R. A., G. M. Heymsfield, and J. Hallett, 2003: Extra large particle images at 12 km in a hurricane eyewall: Evidence of high-altitude supercooled water? *Geophys. Res. Lett.,* **30,** 2124, doi:10.1029/2003GL017864.

Carroll, B. J., 1976: The accurate measurement of contact angle, phase contact areas, drop volume, and Laplace excess pressure in drop-on-fiber systems. *J. Colloid Interface Sci.,* **57** (3), 488–495.

Clough, S. A., and A. A. Franks, 1991: The evaporation of frontal and other stratiform precipitation. *Quart. J. Roy. Meteor. Soc.,* **117,** 1057–1080.

——, H. W. Lean, N. M. Roberts, and R. M. Forbes, 2000: Dynamical effects of ice sublimation in a frontal wave. *Quart. J. Roy. Meteor. Soc.,* **126,** 2405–2434.

Dong, Y. Y., R. G. Oraltay, and J. Hallett, 1994: Ice particle generation during evaporation. *Atmos. Res.,* **32,** 45–53.

Drummond, F. J., R. R. Rogers, S. A. Cohn, W. L. Eckland, D. A.

Carter, and J. S. Wilson, 1996: A new look at the melting layer. *J. Atmos. Sci.,* **53,** 759–769.

Fabry, F., and W. Szyrmer, 1999: Modeling of the melting layer. Part II: Electromagnetic. *J. Atmos. Sci.,* **56,** 3593–3600.

Furukawa, Y., M. Yamamoto, and T. Kuroda, 1987: Ellipsometric study of the transition layer on the surface of an ice crystal. *J. Cryst. Growth,* **82,** 665–667.

Hallett, J., and B. J. Mason, 1958: The influence of temperature and supersaturation on the habit of ice crystals grown from the vapour. *Proc. Roy. Soc. of London,* **A247,** 440–453.

Johnson, D., and J. Hallett, 1968: Freezing and shattering of supercooled water drops. *Quart. J. Roy. Meteor. Soc.,* **94,** 468–482.

Kamburova, P. L., and F. H. Ludlam, 1966: Rainfall evaporation in thunderstorm downdraughts. *Quart. J. Roy. Meteor. Soc.,* **92,** 510–518.

Keller, V. W., and J. Hallett, 1982: Influence of air velocity on the habit of ice crystal growth from the vapor. *J. Cryst. Growth,* **60,** 91–106.

Knight, C. A., 1979: Observations of the morphology of melting snow. *J. Atmos. Sci.,* **36,** 1123–1130.

Matsuo, T., and Y. Sasyo, 1981: Melting of snowflakes below the freezing level in the atmosphere. *J. Meteor. Soc. Japan,* **59,** 10–24.

Mitra, S. K., O. Vohl, M. Ahr, and H. R. Pruppacher, 1990: A wind tunnel and theoretical study of the melting behavior of atmospheric ice particles. IV: Experiment and theory for snowflakes. *J. Atmos. Sci.,* **47,** 584–591.

Mittermaier, M. P., and A. J. Illingworth, 2003: Comparison of model-derived and radar-observed freezing level heights: Implications for vertical reflectivity profile correction schemes. *Quart. J. Roy. Meteor. Soc.,* **129,** 83–95.

Oraltay, R. G., and J. Hallett, 1989: Evaporation and melting of ice crystals: A laboratory study. *Atmos. Res.,* **24,** 169–189.

Stewart, R. E., 1984: Deep isothermal layers within precipitation bands over southern Ontario. *J. Geophys. Res.,* **89,** 2567–2572.

——, J. D. Marwitz, J. C. Pace, and R. E. Carbone, 1984: Characteristics through the melting layer of stratiform clouds. *J. Atmos. Sci.,* **41,** 3227–3237.

Szyrmer, W., and I. Zawadzki, 1999: Modeling of the melting layer. Part I: Dynamics and microphysics. *J. Atmos. Sci.,* **56,** 3573–3592.

Willis, P., and A. J. Heymsfield, 1989: Structure of the melting layer in mesoscale convective system stratiform precipitation. *J. Atmos. Sci.,* **46,** 2008–2025.